Scalable Parallel Screening of Catalyst Activity at the Single-Particle Level and Subdiffraction Resolution

Xiaochun Zhou, Eric Choudhary, Nesha May Andoy,[†] Ningmu Zou, and Peng Chen*

Department of Chemistry and Chemical Biology, Cornell University, Ithaca, New York 14853, United States

Ⓢ *Supporting Information*

ABSTRACT: High-throughput and quantitative screening of catalyst activity is crucial for guiding the work cycles of catalyst improvements and optimizations. For nanoparticle catalysts, their inherent heterogeneity makes it desirable to screen them at the single-particle level. Here, we report a single-molecule fluorescence microscopy approach that can screen the activity quantitatively of a large number of catalyst particles in parallel at the single-particle level and with subdiffraction spatial resolution. It can identify directly high activity catalyst particles and resolve subpopulations in mixtures of catalysts. It is readily scalable and broadly applicable to heterogeneous catalysts. Using ensemble measurements to establish activity correlations between different reactions, we further show that this approach can be extended to assess catalysts in reactions that do not involve fluorescent molecules. Coupled with high-throughput catalyst preparation and high-resolution structural/compositional analysis, this screening approach has promise in accelerating the development and discovery of new or better catalysts.

KEYWORDS: *heterogeneous catalysis, single-molecule imaging, deoxygenation, deacetylation, nitro-reduction, phenol oxidation*
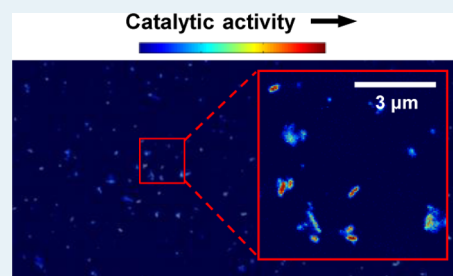
1. INTRODUCTION

Nanoparticles are among the most important industrial catalysts. They can be made of many different materials, such as metals and metal oxides, and can catalyze a variety of chemical transformations. Developing better and less expensive nanoparticle catalysts remains a major goal of catalysis research. Many efforts have been directed to making nanoparticles of various morphologies and compositions. For example, advances in colloidal chemistry have made it possible to prepare nanoparticles of well-controlled size, shape, and composition, in which the shape control renders the control of surface facets.[1−5] Parallel methods[6] have also been developed that can produce nanoparticles[7] or (electro)catalysts of tremendous diversity in composition and structure for catalyzing reactions such as hydrogen oxidation,[8] thiophene oxidation,[9] fuel cell reactions,[10−15] gasoline processing,[16] and photocatalysis[17] (see also reviews 18 and 19).

Regardless of their preparation methods, precisely controlled or diversity-oriented, nanoparticle catalysts always need to be screened in reaction measurements to confirm or test their catalytic activity in various chemical transformations of interest. Here, high-throughput and quantitative methods are always desirable to quickly feed the activity information back to the next round of catalyst improvements and optimizations. To this end, thermographic imaging,[8] laser-induced resonance-enhanced multiphoton ionization,[20] fluorescence microscopy,[10,12,21,22] scanning electrochemical microscopy (SECM),[11−13,15,17] and multichannel reactor vessels[16] have been used to screen the catalyst activity in parallel.

Moreover, the activity screening of nanoparticle catalysts is preferentially done at the single-particle level because, above all,

they are highly heterogeneous.[23−26] Even for size- and shape-controlled nanocrystals, individual particles differ from one another. For diversity-orientated preparations, the catalyst heterogeneity is more pronounced. Several approaches that are capable of studying the (electro)catalytic activity of nanoparticles at the single-particle level have been developed. These include scanning probe microscopy (e.g., scanning tunneling microscopy and SECM),[27−31] detecting collision-induced current transients on microelectrodes,[32−36] using single particles as electrodes,[37−40] and localized surface plasmon resonance (LSPR) microscopy.[41−46] Although powerful, each has limitations: the scanning probe approaches have low data throughput; the electrical-current-based measurements not only have low data throughput but also are limited to electrocatalysts; the LSPR microscopy is generally limited to plasmonic metal catalysts and has diffraction-limited spatial resolution (about 200−300 nm).

Single-molecule fluorescence microscopy recently has emerged as an effective approach to study catalytic reactions on individual catalyst particles.[26,47−51] In this approach, a fluorogenic reaction is used, and fluorescence microscopy is used to detect the fluorescence signal of a reaction product on immobilized catalyst particles at the single-molecule level (Figure 1A). Quantitative activity of single catalyst particles can be obtained readily. With sufficient fluorescence signals, the positions of individual product molecules can further be localized to nanometer precision,[52,53] allowing imaging beyond
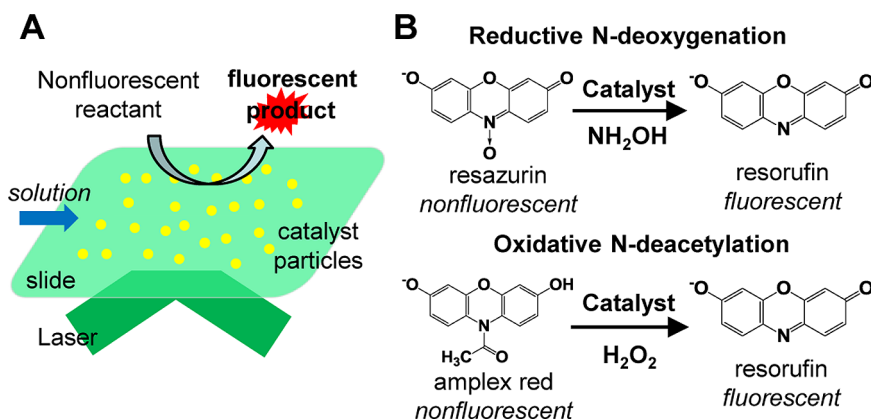
Figure 1. Single-molecule fluorescence microscopy of fluorogenic reactions. (A) Schematic of using wide-field total internal reflection fluorescence microscopy to image fluorogenic catalytic reactions by a large number of catalyst particles immobilized on a quartz slide. The reactant solution is supplied in a continuous flow in a microfluidic reactor, resulting in steady-state reaction kinetics. (B) The two fluorogenic probe reactions for catalysis: a reductive N-deoxygenation of resazurin to resorufin by NH_2OH, and an oxidative N-deacetylation of amplex red to resorufin by H_2O_2.

the diffraction-limited resolution to tens of nanometers (i.e., subdiffraction resolution).[50,54−64]

Here, we demonstrate that this single-molecule subdiffraction imaging approach can be scaled up to screen the activity of a large number of catalyst particles in parallel. Quantitative activity can be obtained at the single-particle level that enables identification of high activity particles. By using activity correlations between different reactions, we further show that this approach can assess catalyst activity beyond fluorogenic reactions. Coupled with high-throughput synthetic methods of catalysts and high-resolution structural and compositional analysis, this approach has the potential to accelerate catalyst development and discovery.

2. MATERIALS AND METHODS

Catalyst preparation/characterization, single-molecule fluorescence microscopy, ensemble activity assays, and data analysis are described in the Supporting Information (SI), sections S1−S3. All catalysis experiments were performed at room temperature in aqueous solution.

3. RESULTS AND DISCUSSIONS

3.1. Single-Molecule Subdiffraction Imaging of Single-Particle Catalysis. We first demonstrate the subdiffraction spatial resolution of our approach in imaging catalysis on single catalyst particles. To do so, we used two types of pseudospherical particles as model catalysts. One type is bare Au particles of 6−14 nm in diameter (here "bare" means that they do not have strong capping ligands such as CTAB or additional shells); the other is mesoporous silica-coated Au particles (i.e., Au@mSiO$_2$ particles) with variable core diameters and shell thicknesses (SI, Table S1). We used two fluorogenic reactions as our probe catalytic reactions: one a reductive N-deoxygenation of resazurin to resorufin by NH_2OH and the other an oxidative N-deacetylation of amplex red to resorufin by H_2O_2. Resorufin is a highly fluorescent molecule (Figure 1B). Using wide-field total-internal-reflection single-molecule fluorescence microscopy, we imaged and localized the product molecules catalytically generated on individual particles one at a time in real time (Figure 1A).

Figure 2A shows the locations of the catalytic products from a single 6-nm bare Au particle catalyzing the N-deoxygenation reaction. The fwhm of the 2-D histogram of these locations is

∼30 nm (Figure 2B, and SI Figure S9C), which is 10 times smaller than the diffraction-limited resolution (∼300 nm). Because this 2-D histogram can be plotted in an image format (i.e., Figure 2B), we refer to this type of plot as "subdiffraction catalysis images". Nevertheless, the object in Figure 2B is still larger than the physical size of the 6-nm particle, which reflects the resolution limit of our approach. Depending on the number of the detected fluorescence photons of individual catalytic products, our effective spatial resolution is ∼15 nm at best, but is typically 30−40 nm when all product molecules that differ in photon counts are included in the analysis (SI, section S4). Consistent with this spatial resolution, for a pseudospherical Au@mSiO$_2$ particle that is significantly larger than our spatial resolution, the fwhm of the 2-D histogram of its product locations is about the same as its physical size (Figure 2C, D).

Knowing the effective spatial resolution of our approach, we used three analysis methods to extract the apparent sizes of individual catalyst particles from their subdiffraction catalysis images over a series of Au and Au@mSiO$_2$ particles. One method involves fitting the data with a model; the other two use empirical fittings (details in the SI, section S4). Figure 2E plots the apparent sizes of these particles from the subdiffraction catalysis imaging against their diameters determined from TEM. For larger particles, their apparent sizes are about the same as their true physical sizes. With decreasing particle size to smaller than 30−40 nm, the apparent sizes from subdiffraction catalysis imaging deviate toward the larger side of the true sizes and eventually flatten out to a limiting value, which reflects our approach's resolution limit. Overall, these results demonstrate that we can image the catalysis of individual catalyst particles at tens of nanometer resolution, that is, subdiffraction resolution.

3.2. Screening Mixtures of Pseudospherical Au@mSiO$_2$ Particles. To demonstrate that our approach is capable of screening and differentiating the activities of a large number of catalyst particles in parallel, we applied it to a mixture of 21@42 nm and 102@32 nm pseudospherical Au@mSiO$_2$ particles (SI, Table S1). Figure 3A presents the subdiffraction catalysis image of ∼1000 particles on a slide in catalyzing the N-deoxygenation reaction, alongside the SEM image of the same sample (Figure 3B). Individual particles are clearly resolved in the subdiffraction catalysis image, including those within aggregates (Figure 3A, inset). More important, this subdif-
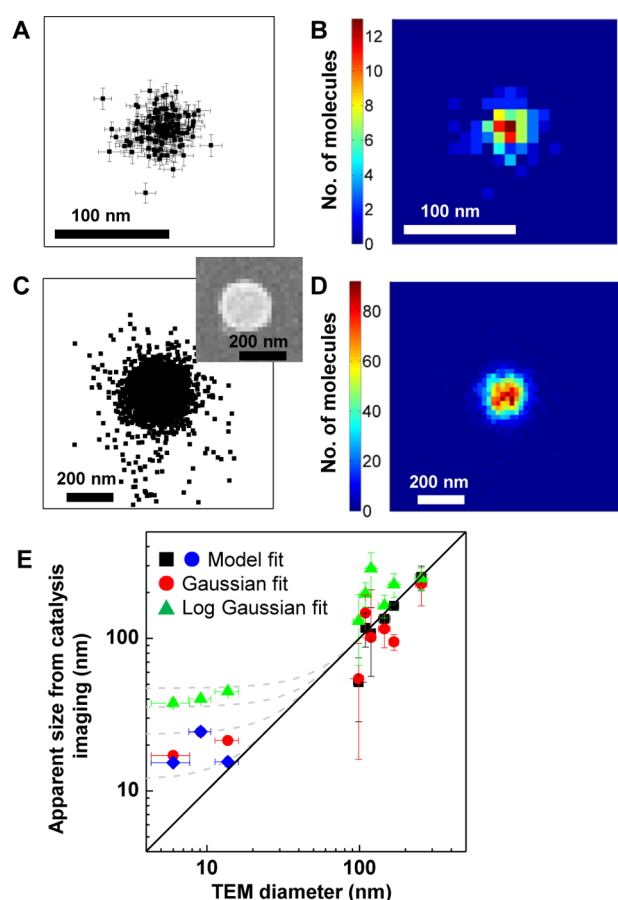
Figure 2. Single-molecule subdiffraction imaging of single-particle catalysis. (A) Locations of 141 product molecules from a 6-nm bare Au particle catalyzing the N-deoxygenation reaction of resazurin. (B) Image plot of the 2-D histogram of A with 10×10 nm^2 bin. (C, D) Same as A and B, but for a 102@33 nm (core-diameter@shell-thickness) Au@mSiO$_2$ particle with ~4900 product molecules in catalyzing the N-deacetylation reaction of amplex red. Inset in C is the particle's SEM image. (E) Correlation between the TEM (outer) diameter and the apparent size from subdiffraction catalysis imaging over a series of catalyst samples. The apparent sizes from the subdiffraction catalysis imaging are extracted using three different methods, as described in the SI, section S4. These methods are referred to as model fit, Gaussian fit, and log Gaussian fit, respectively. Each data point is an average of many particles in one catalyst sample. The catalyst samples here include pseudospherical bare Au particles 6, 9, and 14 nm in diameter, and Au@mSiO$_2$ particles 42@28, 42@38, 60@25, 60@42, 60@97, and 102@33 nm in size. The four dashed lines are simulations assuming that reactions occur evenly on a spherical surface of a certain diameter; the resulting product distributions on the spheres are then projected into 2-D or 1-D and further convoluted with a Gaussian broadening function that has a standard deviation of 10, 15, 20, or 25 nm, respectively. The FWHMs of the convoluted distribution functions are then plotted here. See simulation details in the SI, section S4.1. Error bars are all standard deviations.

fraction catalysis image immediately reports the activities of individual particles, quantified by the number of product molecules detected on them. For example, particle 1 is clearly more active than particle 2 because it generated more product molecules during the same reaction time (Figure 3A inset), even though the two particles are similar in size (Figure 3B, inset). Overall, large heterogeneity in activity is clear among

individual particles, which corroborates the need for single-particle level screening.

Pooling the results from many particles together, we obtained the distributions of their sizes and activities (Figure 3C, D and the SI, section S5). Here, the activities are represented by v, the rate of turnovers per particle. We also excluded the aggregates in these distributions for convenience in automated data analysis. Two subpopulations are clear in the 2-D histogram of size and activity, corresponding to the 21@42 nm and 102@32 nm Au@mSiO$_2$ particles (Figure 3D). The larger 102@32 nm particles have higher activity, likely due to their larger Au surface areas per particle.

Among all particles in this mixture, the general trend is, unsurprisingly, that larger particles are more active on a per-particle basis, with a Pearson's correlation coefficient of ~0.68 between size and activity (Figure 3C). However, some smaller particles show significantly higher activities (e.g., particle 3, Figure 3C), whereas some larger ones show lower activities (e.g., particle 7, Figure 3C), compared with those of similar sizes. This direct identification of catalyst activity at the single-particle level is exciting because one can now pinpoint the particle of desired activity for subsequent structural characterizations, although our structural characterization is currently just at the SEM level, which is insufficient to identify the structural basis of activity differences (Figure 3C insets).

We also examined this mixture of the two types of Au@ mSiO$_2$ particles in catalyzing the N-deacetylation reaction. We again were able to screen and quantify the activity of a large number of particles in parallel at the single-particle level and subdiffraction resolution, as well as resolve their subpopulations (Figure 3E, F, and the SI, section S6).

3.3. Screening Mixtures of Different-Shaped Catalyst Particles. Here, we demonstrate that our approach can screen and differentiate the activity of not only mixtures of different-sized catalyst particles, but also mixtures of different-shaped ones. We used a mixture of Au@mSiO$_2$ particles with pseudospherical, triangular, and rod-shaped Au cores as our model catalysts (SI, Figure S3) in catalyzing the N-deacetylation reaction of amplex red. Because of the mSiO$_2$ shell, those with small triangular cores are difficult to distinguish by shape in SEM from those with pseudospherical cores. We thus grouped them together as "pseudo-spherical" particles that have two subpopulations differing in size (outer diameter: 158.3 ± 47.0 nm and 243.3 ± 44.5 nm; the larger ones are those with triangular cores; SI, Figure S25B). The Au@mSiO$_2$ rods are ~160 nm in outer diameter and have outer lengths ranging from ~260 to ~860 nm, as we previously reported[62] (SI, Figure S25A).

Figure 4A shows the subdiffraction catalysis image of ~900 of these differently shaped catalyst particles, alongside the SEM image of the same sample (Figure 4B). Individual catalyst particles, as well as their pseudosphere or rod shapes, are clearly resolved in the subdiffraction catalysis image, even within aggregates. Again, the most important information from the subdiffraction catalysis image is the catalytic activities of individual particles, reflected by the number of reaction products detected on them. A large heterogeneity of activity is clear among particles: even for those of similar sizes, some are more active and some less (e.g., particle 12 vs particle 13 in Figure 4A inset). This large activity heterogeneity again corroborates the need for single-particle level activity screening.

We further analyzed the pseudospherical and rod-shaped particles separately. Figure 4C shows the distribution of size
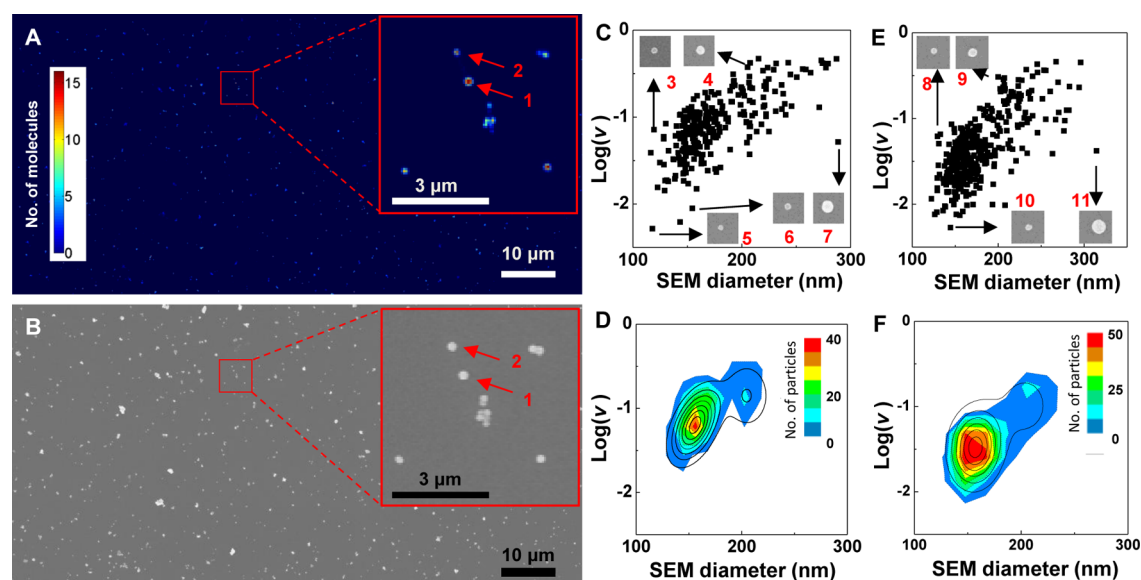
Figure 3. Parallel activity screening of a mixture of pseudospherical 21@42 nm and 102@32 nm Au@mSiO$_2$ particles. (A) Subdiffraction catalysis image of ~1000 particles in catalyzing the reductive N-deoxygenation of resazurin to resorufin. This image is generated with 20 × 20 nm^2 bins. Inset: a zoom-in. Reaction conditions in the SI, section S5. (B) SEM image of the same set of particles as in A with a zoom-in inset. (C) Scatter plot of individual catalyst particles against their respective SEM diameters and rates of turnovers (v, in s^{-1} particle^{-1} in log scale) from A and B. Each point represents one particle. Insets: SEM images of selected particles. (D) Contour plot of the 2-D histogram of C. Bin size: 20 nm ×0.25. The solid black lines are fits with two 2-D Gaussian functions. (E, F) Same as C and D , but for a different batch of samples in catalyzing the oxidative N-deacetylation of amplex red to resorufin. Reaction conditions are in the SI, section S6.

and activity of the pseudospherical catalyst particles (we again excluded those in aggregates for convenience in data analysis; see also the SI, section S7). Two subpopulations are clearly resolved in the distribution, with the larger particles having higher activities on a per-particle basis. Figure 4D shows the correlation between activity and aspect ratio of individual rods. Here, no clear subpopulations are visible, although large activity heterogeneity is apparent. This direct identification of catalyst activity at the single-particle level again allows us to pinpoint specific particles of high or low activity, for example, those in the Figure 4D insets.

3.4. Activity Correlation between Fluorogenic Probe Reactions and Common Model Redox Reactions. For our imaging approach, one of the catalytic products needs to be fluorescent. Therefore, catalytic reactions that do not generate fluorescent molecules cannot be studied directly. However, the types of chemical transformations to be studied are not limited because one can design reactant molecules that undergo the desired chemical transformation to generate a fluorescent molecule. For example, the two fluorogenic probe reactions we use here represent distinct chemical transformations: one an N-deacetylation reaction and the other an N-deoxygenation reaction (Figure 1B).

On the other hand, one may *not* even need to design new fluorogenic reactions for screening catalysts for a particular chemical transformation. Our hypothesis is the following: If a catalyst's activity in a reaction of interest is well correlated with its activity in either of the two fluorogenic probe reactions we study here, then our fluorescence microscopy-based screening results can be used to predict the (relative) activity of catalyst particles in the reaction of interest. Here, we demonstrate such activity correlations between the two fluorogenic probe reactions and two common model reactions for studying catalysts.

The two model reactions we chose are the reduction of 4-nitrophenol to 4-aminophenol and the oxidation of hydroquinone to quinone (SI, Figure S29 and section S8). Both are commonly used to test the activity of catalysts.[65] We tested two series of catalysts: one bare pseudospherical Au particles and the other pseudospherical Au@mSiO$_2$ particles, both of varying sizes (SI, Table S1). Figure 5A shows the correlation between the activities of these catalysts in 4-nitrophenol reduction and in resazurin N-deoxygenation. Figure 5B shows the correlation between their activities in hydroquinone oxidation and in amplex red N-deacetylation. In both cases, linear positive correlation is observed: when a catalyst is high in activity in the reductive N-deoxygenation reaction of resazurin, it is also high in activity in the 4-nitrophenol reduction reaction, and when a catalyst is high in activity in the oxidative N-deacetylation reaction of amplex red, it is also high in activity in the hydroquinone oxidation reaction. The correlation coefficients are all ~1.0, even though the activities of the catalyst particles vary over many orders of magnitude. These correlations demonstrate that for the 4-nitrophenol reduction and hydroquinone oxidation reactions, even though we cannot directly screen the catalyst activities using our single-molecule imaging approach, we can still screen them at the single-particle level using our fluorogenic probe reactions to obtain equivalent information. This correlation approach can be broadly applied to many other catalytic reactions; one just needs to establish their correlations with a fluorogenic reaction using conventional ensemble measurements before applying the single-molecule fluorescence microscopy approach for activity screening at the single-particle level.

4. CONCLUDING REMARKS

We have shown here that the single-molecule fluorescence microscopy approach offers a quantitative way to screen the activity of a large number of catalyst particles in parallel at the
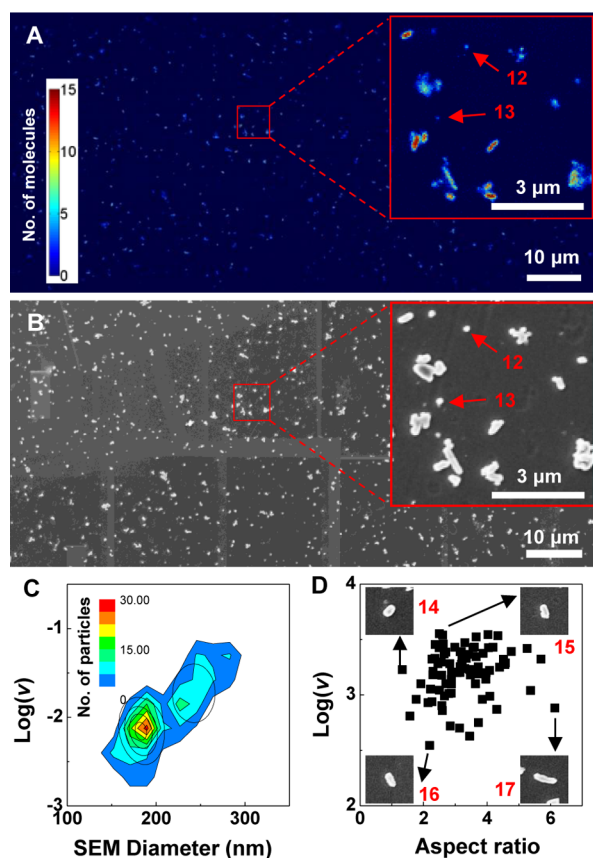
Figure 4. Parallel activity screening of a mixture of pseudospherical and rod-shaped Au@mSiO$_2$ particles in catalyzing the oxidative N-deacetylation of amplex red to resorufin. Reaction conditions are in the SI, section S7. (A) Subdiffraction catalysis image of ~900 particles with a zoom-in inset. Image generated with 20 × 20 nm^2 bins. (B) SEM image of the same set of particles as in A with a zoom-in inset. (C) Contour plot of the 2-D histogram of ~220 pseudospherical particles against their respective SEM diameters and rates of turnovers (ν, in s^{-1} particle^{-1} in log scale) from A and B. Bin size: 20 nm ×0.25. The solid black lines are fits with two 2-D Gaussian functions (also SI, Figure S26 and section S7). (D) Scatter plot of ~80 rods from A and B against their respective aspect ratios (from SEM image) and log(ν). Insets: SEM images of selected rods.

single-particle level and subdiffraction resolution. This approach is applicable to many types of (nano)catalysts, and the results can be extrapolated using activity correlations to evaluate catalyst activity beyond fluorogenic reactions. With motorized fluorescence microscopes and larger camera formats, this approach can be scaled up significantly to identify highly active ones among many thousands of catalyst particles, which can then be selected for subsequent high-resolution structural and compositional analysis, for example, using high-resolution electron microscopy.[66] Coupled with combinatorial or parallel synthesis of catalysts,[6–12,16,17] one can envision that this approach will be powerful for assessing catalyst synthesis protocols and the performance of resulting catalysts. The information can then be fed back quickly to the next round of catalyst synthesis and optimization, which would accelerate the discovery and development of new or better catalysts.
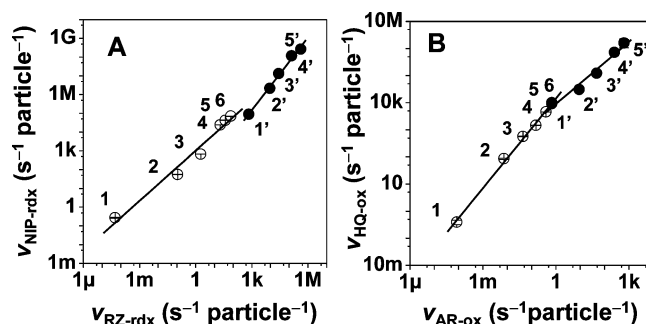

Figure 5. Activity correlation for the same sets of catalyst particles between different reactions. (A) Correlation between the reductive N-deoxygenation reaction of resazurin (i.e., RZ-rdx) and the reduction of 4-nitrophenol (i.e., NIP-rdx). For bare Au particles, the correlation coefficient is $\rho \sim 1.00$; for Au@mSiO$_2$ particles, $\rho \sim 0.99$. (B) Correlation between the oxidative N-deacetylation reaction of amplex red (i.e., AR-ox) and the oxidation of hydroquinone (i.e., HQ-ox). For bare Au particles, $\rho \sim 0.98$; for Au@mSiO$_2$ particles, $\rho \sim 1.00$. All error bars are standard deviations. Solid lines are linear fits. The activities were measured at the ensemble level and quantified by the rate of turnovers, ν, in s^{-1} particle^{-1}. Two series of catalyst particles were tested (SI, Table S1): one (●), bare pseudospherical Au particles 6, 9, 21, 102, and 226 nm in diameter, denoted as 1′, 2′, 3′, 4′, and 5′; the other (○), pseudospherical Au@mSiO$_2$ particles of 6@38, 21@81, 42@65, 42@70, 60@83, 102@59 nm in size, denoted as 1, 2, 3, 4, 5, and 6, in the plots.

■ ASSOCIATED CONTENT

Ⓢ Supporting Information

Details of catalyst preparation and characterization procedures, single-molecule fluorescence microscopy, ensemble activity assays, data analysis, and supporting figures and tables. This material is available free of charge via the Internet at http://pubs.acs.org.

■ AUTHOR INFORMATION

Corresponding Author
*Phone: 607-254-8533. E-mail: pc252@cornell.edu.

Present Address
†(Nesha May Andoy) Department of Cell Biology, Harvard Medical School, Boston, MA 02115, USA

Notes
The authors declare the following competing financial interest(s): The authors have filed an invention disclosure based on the work described in this manuscript.

■ REFERENCES

(1) Habas, S. E.; Lee, H.; Radmilovic, V.; Somorjai, G. A.; Yang, P. Nat. Mater. **2007**, 6, 692.
(2) Ahmadi, T. S.; Wang, Z. L.; Green, T. C.; Henglein, A.; El-Sayed, M. A. Science **2006**, 272, 1924.
(3) Sun, Y.; Xia, Y. Science **2002**, 298, 2176.

(4) Millstone, J. E.; Hurst, S. J.; Métraux, G. S.; Cutler, J. I.; Mirkin, C. A. *Small* **2009**, *5*, 646.

(5) Murphy, C. J.; Thompson, L. B.; Chernak, D. J.; Yang, J. A.; Sivapalan, S. T.; Boulos, S. P.; Huang, J.; Alkilany, A. M.; Sisco, P. N. *Curr. Opin. Colloid Interface Sci.* **2011**, *16*, 128.

(6) Hanak, J. J. *J. Mater. Sci.* **1970**, *5*, 964.

(7) Salaita, K.; Wang, Y.; Fragala, J.; Vega, R. A.; Liu, C.; Mirkin, C. A. *Angew. Chem., Int. Ed.* **2006**, *45*, 7220.

(8) Moates, F. C.; Somani, M.; Annamalai, J.; Richardson, J. T.; Luss, D.; Willson, R. C. *Ind. Eng. Chem. Res.* **1996**, *35*, 4801.

(9) Hill, C. L.; Gall, R. D. *J. Mol. Catal. A* **1996**, *114*, 103.

(10) Reddington, E.; Sapienza, A.; Gurau, B.; Viswanathan, R.; Sarangapani, S.; Smotkin, E. S.; Mallouk, T. E. *Science* **1998**, *280*, 1735.

(11) Fernandez, J. L.; Walsh, D. A.; Bard, A. J. *J. Am. Chem. Soc.* **2005**, *127*, 357.

(12) Prochaska, M.; Jin, J.; Rochefort, D.; Zhuang, L.; DiSalvo, F. J.; Abruña, H. D.; van Dover, R. B. *Rev. Sci. Instrum.* **2006**, *77*, 054104.

(13) Jin, J.; Prochaska, M.; Rochefort, D.; Kim, D. K.; Zhuang, L.; DiSalvo, F. J.; Van Dover, R. B.; Abruna, H. D. *Appl. Surf. Sci.* **2007**, *254*, 653.

(14) Prochaska, M.; Jin, J.; Rochefort, D.; Zhuang, L.; DiSalvo, F. J.; Abruna, H. D.; van Dover, R. B. *Rev. Sci. Instrum.* **2006**, *77*.

(15) Gregoire, J. M.; Kostylev, M.; Tague, M. E.; Mutolo, P. F.; van Dover, R. B.; DiSalvo, F. J.; Abruna, H. D. *J. Electrochem. Soc.* **2009**, *156*, B160.

(16) Turner, H. W.; Volpe, A. F., Jr.; Weinberg, W. H. *Surf. Sci.* **2009**, *603*, 1763.

(17) Jang, J. S.; Lee, J.; Ye, H.; Fan, F.-R. F.; Bard, A. J. *J. Phys. Chem. C* **2009**, *113*, 6719.

(18) Weinberg, W. H.; Jandeleit, B.; Self, K.; Turner, H. *Curr. Opin. Solid State Mater. Sci.* **1998**, *3*, 104.

(19) McFarland, E. W.; Weinberg, W. H. *Trends Biotechnol.* **1999**, *17*, 107.

(20) Senkan, S. M. *Nature* **1998**, *394*, 350.

(21) Guerrette, J. P.; Percival, S. J.; Zhang, B. *J. Am. Chem. Soc.* **2013**, *135*, 855.

(22) Leenheer, A. J.; Atwater, H. A. *J. Electrochem. Soc.* **2012**, *159*, H752.

(23) Weckhuysen, B. M. *Angew. Chem., Int. Ed.* **2009**, *48*, 4910.

(24) Buurmans, I. L. C.; Weckhuysen, B. M. *Nat. Chem.* **2012**, *4*, 873.

(25) Grunwaldt, J.-D.; Wagner, J. B.; Dunin-Borkowski, R. E. *ChemCatChem* **2013**, *5*, 62.

(26) Xu, W.; Kong, J. S.; Yeh, Y.-T. E.; Chen, P. *Nat. Mater.* **2008**, *7*, 992.

(27) Meier, J.; Friedrich, K. A.; Stimming, U. *Faraday Discuss.* **2002**, *121*, 365.

(28) Tel-Vered, R.; Bard, A. J. *J. Phys. Chem. B* **2006**, *110*, 25279.

(29) Nakai, M.; Yamanoi, Y.; Nishimori, Y.; Yonezawa, T.; Nishihara, H. *Angew. Chem., Int. Ed.* **2008**, *47*, 6699.

(30) Sánchez-Sánchez, C. M.; Solla-Gullón, J.; Vidal-Iglesias, F. J.; Aldaz, A.; Montiel, V.; Herrero, E. *J. Am. Chem. Soc.* **2010**, *132*, 5622.

(31) Lai, S. C. S.; Dudin, P. V.; Macpherson, J. V.; Unwin, P. R. *J. Am. Chem. Soc.* **2011**, *133*, 10744.

(32) Xiao, X.; Bard, A. J. *J. Am. Chem. Soc.* **2007**, *129*, 9610.

(33) Fan, F.-R. F.; Bard, A. J. *Nano Lett.* **2008**, *8*, 1746.

(34) Xiao, X.; Fan, F.-R. F.; Zhou, J.; Bard, A. J. *J. Am. Chem. Soc.* **2008**, *130*, 16669.

(35) Xiao, X.; Pan, S.; Jang, J. S.; Fan, F.-R. F.; Bard, A. J. *J. Phys. Chem. C* **2009**, *113*, 14978.

(36) Kwon, S. J.; Fan, F.-R. F.; Bard, A. J. *J. Am. Chem. Soc.* **2010**, 13165−13167.

(37) Chen, S.; Kucernak, A. *J. Phys. Chem. B* **2004**, *108*, 13984.

(38) Murray, R. W. *Chem. Rev.* **2008**, *108*, 2688.

(39) Krapf, D.; Wu, M.-Y.; Smeets, R. M. M.; Zandbergen, H. W.; Dekker, C.; Lemay, S. G. *Nano Lett.* **2006**, *6*, 105.

(40) Li, Y.; Cox, J. T.; Zhang, B. *J. Am. Chem. Soc.* **2010**, *132*, 3047.

(41) Novo, C.; Funston, A. M.; Mulvaney, P. *Nat. Nanotechnol.* **2008**, *3*, 598.

(42) Novo, C.; Funston, A. M.; Gooding, A. K.; Mulvaney, P. *J. Am. Chem. Soc.* **2009**, *131*, 14664.

(43) Cheng, J.; Liu, Y.; Cheng, X.; He, Y.; Yeung, E. S. *Anal. Chem.* **2010**, *82*, 8744.

(44) Tang, M. L.; Liu, N.; Dionne, J. A.; Alivisatos, A. P. *J. Am. Chem. Soc.* **2011**, *133*, 13220.

(45) Liu, N.; Tang, M. L.; Hentschel, M.; Giessen, H.; Alivisatos, A. P. *Nat. Mater.* **2011**, *10*, 631.

(46) Shan, X.; Díez-Pérez, I.; Wang, L.; Wiktor, P.; Gu, Y.; Zhang, L.; Wang, W.; Lu, J.; Wang, S.; Gong, Q.; Li, J.; Tao, N. *Nat. Nanotechnol.* **2012**, *7*, 668.

(47) De Cremer, G.; Sels, B. F.; Vos, D. E. D.; Hofkens, J.; Roeffaers, M. B. J. *Chem. Soc. Rev.* **2010**, *39*, 4703.

(48) Chen, P.; Zhou, X.; Shen, H.; Andoy, N. M.; Choudhary, E.; Han, K.-S.; Liu, G.; Meng, W. *Chem. Soc. Rev.* **2010**, *39*, 4560.

(49) Tachikawa, T.; Majima, T. *Chem. Soc. Rev.* **2010**, *39*, 4802.

(50) Roeffaers, M. B.; Sels, B. F.; Uji-i, H.; De Schryver, F. C.; Jacobss, P. A.; De Vos, D. E.; Hofkens, J. *Nature* **2006**, *439*, 572.

(51) Naito, K.; Tachikawa, T.; Fujitsuka, M.; Majima, T. *J. Am. Chem. Soc.* **2009**, *131*, 934.

(52) Yildiz, A.; Forkey, J. N.; McKinney, S. A.; Ha, T.; Goldman, Y. E.; Selvin, P. R. *Science* **2003**, *300*, 2061.

(53) Thompson, R. E.; Larson, D. R.; Webb, W. W. *Biophys. J.* **2002**, *82*, 2775.

(54) Roeffaers, M. B. J.; Hofkens, J.; De Cremer, G.; De Schryver, F. C.; Jacobs, P. A.; De Vos, D. E.; Sels, B. F. *Catal. Today* **2007**, *126*, 44.

(55) Roeffaers, M. B.; De Cremer, G.; Uji-i, H.; Muls, B.; Sels, B. F.; Jacobs, P. A.; De Schryver, F. C.; De Vos, D. E.; Hofkens, J. *Proc. Natl. Acad. Sci. U.S.A.* **2007**, *104*, 12603.

(56) Xu, W.; Shen, H.; Kim, Y. J.; Zhou, X.; Liu, G.; Park, J.; Chen, P. *Nano Lett.* **2009**, *9*, 3968.

(57) Roeffaers, M. B. J.; De Cremer, G.; Libeert, J.; Ameloot, R.; Dedecker, P.; Bons, A.-J.; Buckins, M.; Martens, J. A.; Sels, B. F.; De Vos, D. E.; Hofkens, J. *Angew. Chem., Int. Ed.* **2009**, *48*, 9285.

(58) Tachikawa, T.; Majima, T. *Langmuir* **2009**, *25*, 7791.

(59) De Cremer, G.; Bartholomeeusen, E.; Pescarmona, P. P.; Lin, K.; De Vos, D. E.; Hofkens, J.; Roeffaers, M. B. J.; Sels, B. F. *Catal. Today* **2010**, *157*, 236.

(60) De Cremer, G.; Roeffaers, M. B. J.; Bartholomeeusen, E.; Lin, K.; Dedecker, P.; Pescarmona, P. P.; Jacobs, P. A.; De Vos, D. E.; Hofkens, J.; Sels, B. F. *Angew. Chem., Int. Ed.* **2010**, *49*, 908.

(61) Tachikawa, T.; Yamashita, S.; Majima, T. *J. Am. Chem. Soc.* **2011**, *133*, 7197.

(62) Zhou, X.; Andoy, N. M.; Liu, G.; Choudhary, E.; Han, K.-S.; Shen, H.; Chen, P. *Nature Nanotechnol.* **2012**, *7*, 237.

(63) Tachikawa, T.; Yonezawa, T.; Majima, T. *ACS Nano* **2012**, *7*, 263.

(64) Andoy, N. M.; Zhou, X.; Choudhary, E.; Shen, H.; Liu, G.; Chen, P. *J. Am. Chem. Soc.* **2013**, *135*, 1845.

(65) Hervés, P.; Pérez-Lorenzo, M.; Liz-Marzán, L. M.; Dzubiella, J.; Lu, Y.; Ballauff, M. *Chem. Soc. Rev.* **2012**, *41*, 5577.

(66) Li, Z. Y.; Young, N. P.; Di Vece, M.; Palomba, S.; Palmer, R. E.; Bleloch, A. L.; Curley, B. C.; Johnson, R. L.; Jiang, J.; Yuan, J. *Nature* **2008**, *451*, 46.